https://africanjournalofbiomedicalresearch.com/index.php/AJBR
Afr. J. Biomed. Res. Vol. 27(4s) (November 2024); 18- 42
Research Article

Significance of Solvent Contributions to Thermodynamic Factors, Reactivity Evaluation(ALIE, MEP) , Electronic(UV, TDM, FMO) and Pharmaceutical Applications of 2-Amino-3-Benzyloxypyridine :Anti-Viral Agent

R.M.Indirani[1,2,3], S.K.Geetha[2*], U. Mohamooda Sumaya[4], Jayavelu Udaya Prakash[5], K.Raju[6]

[1]Department of Physics, Bharathi Women's College (Autonomous), Chennai - 600108, Tamil Nadu, India
[2]Department of Physics, Government Arts College for Men (Autonomous), Nandanam, Chennai - 600035, Tamil Nadu, India
[3]University of Madras, Chepauk, Chennai 600 005, Tamil Nadu, India
[4]Department of Physics, R.V. Govt. Arts College, Chengalpattu, Tamil Nadu, India
[5]Department of Mechanical Engineering, Vel Tech Rangarajan Dr. Sagunthala R&D Institute of Science and Technology, Avadi, Chennai 600 062,Tamil Nadu, India
[6]Department of Physics, Easwari Engineering College(Autonomous),Ramapuram, Chennai – 600 089, Tamil Nadu,India

***Corresponding author:** S. K. Geetha
*E-mail address: skgeetha@yahoo.com

Abstract
The organic drug 2-amino-3-benzyloxypyridine has been evaluated theoretically using spectral characterization (FT-IR, FT-Raman, and UV-spectral studies). Electrical characteristics, stability for gas, and different solvents were obtained. Potential Energy Scan carries out structural geometrical specifications and the lowest minimum energy of the compound. Excitation analyses of TDM and UV-Vis spectra demonstrated the stability of the substance. Utilizing the NBO method, the intermolecular dependability of the molecule was ascertained. According to the outcomes, its energy in polar solvents is lower than in non-polar ones, but it is larger in the gas phases compared to the liquid state. Using ELF, LOL, and RDG, the topological behavior of the molecule for gas was investigated. It had been found that the amino acid residues fit well in this ligand. Based on the obtained outcomes, the complex's high energy level gap in the water solvent suggests that it has high chemical stability and low reactivity compared to the other compounds. However, the chloroform and gas phase is the softest and most reactive complex. The study illustrated a drug's biological characteristics and potential for oral usage by using drug-likeness and biological score prediction.

Keyword: DFT, TDM, ALIE, Solvents and Docking

Author for correspondence: Email: skgeetha@yahoo.com

Received: 30 August 2024 *Accepted:05 November 2024*

DOI: https://doi.org/10.53555/AJBR.v27i4S.3489

1. Introduction

The demand for innovative antiviral medications has increased [1]. Aromatic compounds like pyridine are used in many different biological and chemical procedures [2,3]. In addition to other nitrogen dioxide plants, vitamins B3 and B6 also include the pyridine ring molecular motif. Medical evidence indicates that the pyridine nucleus is present in thousands of medications having biological effects [4,5]. A range of fertilizers and insecticides, in addition to a solvent in acrylics and leather goods, are made using pyridine and its byproducts [6]. The practice of DFT may facilitate the development of new microbial inhibitors, spectroscopic techniques [7], and docking to determine a drug's structural action. While spectrum studies and DFT studies have been reported, no spectral research or DFT investigation on pyridine derivatives has been carried out [8,9]. One effective method for examining the various bonding configurations and normal modes of vibration is to employ quantum chemical computations facilitated by DFT in vibrational spectral analysis [10,11]. All vibrational modes have had their complete vibrational assignments supported by potential energy distributions. Theoretical calculations have investigated the 2-amino-3-benzyloxypyridine structure. Theoretical explanations are provided for the 2A3BP FT-IR and FT-Raman spectra. MEP, electrical characteristics, & molecular topologies were examined. As a result, we determined that the theoretical data for the geometrical features (bond-lengths (BL) and bond-angles (BA) agreed well. On a similar theoretical plane, the exchange of charges in the molecular structure is computed using the frontier orbitals technique [12]. The DOS was established to carry out a more comprehensive characterization of the FMOs. In order to characterize intermolecular interactions and to offer details about a molecule's chemical reactivity [13], MEP maps were computed. The reactivity of the chemicals listed can be ascertained with great assistance from all this research. The intermolecular bonds and interaction have been studied with (NBO)[14]. The effectiveness of 2-amino-3-benzyloxypyridines antiviral treatment was evaluated by docking against virus proteins. Docking of molecules was used to figure out the antiviral effect, and the results showed that it may interact irreversibly with the anti-viral proteins.

2. Computational Details

The Gaussian 09W [15] program was implemented for computations using the B3LYP technique [6-311++ G (d,p)] basis set was utilized for computed biophysical parameters. VEDA4 software [16] and PED (Potential Energy Distribution) methodology were used to carry out the vibrational distribution study [17]. UV-Vis, HOMO-LUMO [18], and MEP investigations have been performed utilizing various polar solvents. Atomic bonding and other chemical interactions were studied using ELF. The orbital's impact on the density of states has been determined by the Gauss-Sum program [19]. NBO simulations were performed to investigate the change in electron density between donor and acceptor. To acquire a greater comprehension of the reactive nature of 2A3BP, computed hardness values were evaluated. At the same time, a key parameter, the electrophilicity index, was examined to obtain details about the likely biological activity that occurs [20]. The Multiwfn 3.4.1[21] application was used to investigate charge transfer inside the molecule. The Swiss ADME[22] online program was employed to execute pharmacological property and lipophilicity studies. AutoDock Tools [23] has been employed to investigate molecular docking.

3.Outcome and discussion

3.1. Geometrical Conformations and PES

Figure 1 displays the structure of the optimized molecules of 2-amino-3-benzyloxypyridine. Eleven (C-C), ten (C-H), three (C-N), two (C-O), and two (O-H) bonds, as well as single (O–N, N–H) bond lengths unilaterally were present in the title compound. For 1.5086 Å, the longest bond length occurs at (C4–C5). Furthermore, an appropriate minimum bond length of 1.0098 Å is found in (N3–H26). The greatest possible value of the conspicuous bond angle (123.7366◦) is theoretically detected in (N2–C15–H26), while the minimal angle of bonding are observed to be 103.9607◦ in (O1–C5–H16), respectively. The computational projections for Bond angles and lengths are displayed in Table 1. DFT method predicts that the SCF [24] energy of will be -649.393 Hatrees. SCF Energy = DMF = DMSO = Gas= Methanol = Water › Ethanol › Chloroform. Therefore, based on these findings, we may say that the gas phase tends to be less dependable compared to the solvent. We can confidently state that this method successfully optimized the physical properties of the chosen model of structure [25]. Almost no significant variation existed between polar and non-polar solvents. 37 energy adherents have been identified while analysing the PES, employing rotational angles ranging from 0° to 360° to foresee the stabilized structure shown in Figure 1A. On PES, the stabilized conformer has been detected. The energies of its conformer-I, with angles C6-O1-C5-H17, are -637.89 Hartree. The localized minimum energy of the initial stage (I) of 2A3BP should be provided extra character growth in order to venture its molecular structure and physio-logical qualities.

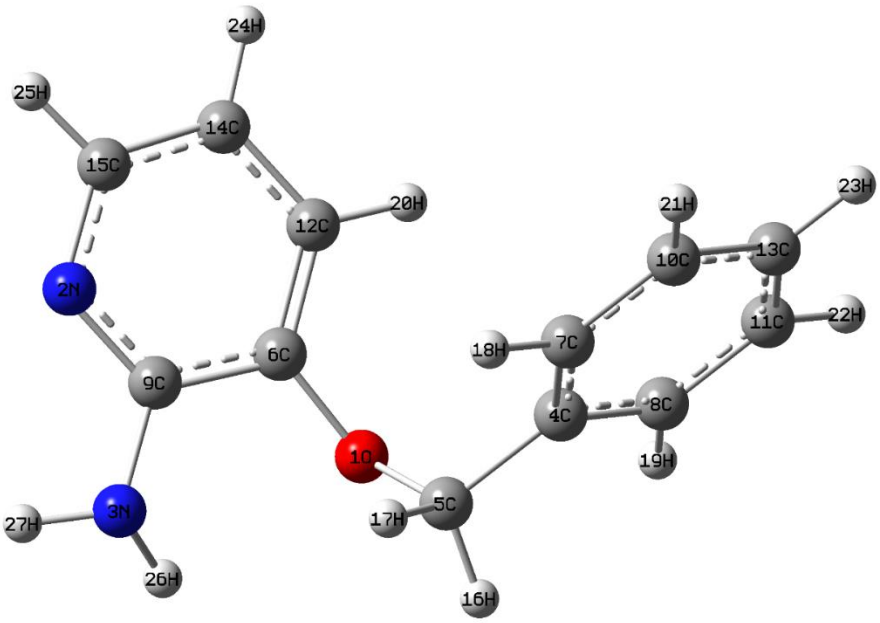

Figure 1. Optimized molecular structure of 2-amino-3-benzyloxypyridine

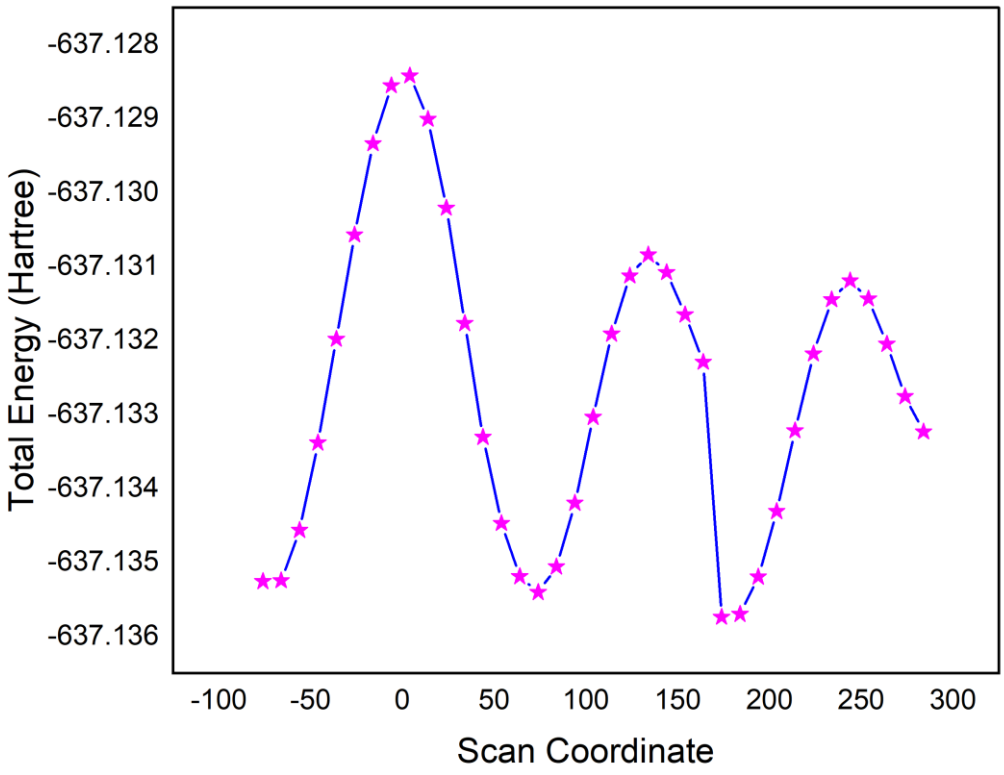

Figure 1 A. PES of 2-amino-3-benzyloxypyridine

Table 1. Bond parameters of 2-amino-3-benzyloxypyridine

Bond Lengths (Å)		**Bond Angles (°)**	
O1-C5	1.4532	C5-O1-C6	115.449
O1-C6	1.3823	C9-N2-C15	118.3237
N2-C9	1.3339	C9-N3-H26	115.5327
N2-C15	1.3387	C9-N3-H27	113.8192
N3-C9	1.3836	H26-N3-H27	115.0848
N3-H26	1.0098	C5-C4-C7	120.9491
N3-H27	1.0099	C5-C4-C8	120.1824
C4-C5	1.5086	C7-C4-C8	118.8678
C4-C7	1.3969	O1-C5-C4	113.2337
C4-C8	1.4003	O1-C5-H16	103.9607
C5-H16	1.0915	O1-C5-H17	109.3695
C5-H17	1.0941	C4-C5-H16	110.6287
C6-C9	1.4146	C4-C5-H17	110.7562
C6-C12	1.3822	H16-5-H17	108.6076
C7-C10	1.3952	O1-C6-C9	118.8317
C7-H18	1.0851	C1-C6-C12	122.2777
C8-C11	1.3916	C9-C6-C12	118.7806
C8-H19	1.0852	C4-C7-C10	120.6741
C10-C13	1.3926	C4-C7-H18	119.5315
C10-H21	1.0843	C10-C7-H18	119.7944
C11-C13	1.3961	C4-C8-C11	120.623
C11-H22	1.0844	C4-C8-H19	119.4562
C12-C14	1.3988	C11-C8-H19	119.9206
C12-H20	1.0833	N2-C9-N3	117.9014
C13-H23	1.0843	N2-C9-C6	122.1121
C14-C15	1.3879	N3-C9-C6	119.9644
C14-H24	1.0828	C7-C10-C13	119.9961
C15-H25	1.0861	C7-C10-H21	119.8618
		C13-C10-H21	120.142
		C8-C11-C13	120.0538
		C8-C11-H22	119.9238
		C13-C11-H22	120.0216
		C6-C12-C14	119.0437
		C6-C12-H20	119.2458
		C14-C12-H20	121.7105

C10-C13-C11	119.7849
C10-C13-H23	120.1295
C11-C13-H23	120.0854
C12-C14-C15	117.9808
C12-C14-H24	121.2269
C15-C14-H24	120.792
N2-C15-C14	123.7366
N2-C15-H25	115.6665
C14-C15-H25	120.5928

3.2. Spectral Vibrational Analysis

Vibrational spectroscopy has shed light on the impact of functional groupings, morphological features, and structural conformation. A molecule with the highest quantity of identifiable functions (N) earns 3 N-6 [26-27]. Three degrees of freedom in rotational & translational. 2A3BP consists of 27 atoms and75 common vibration modes. Computed frequencies were modified using a scaling factor of 0.961[28]. VEDA4 is employed to generate individualised vibrational evaluations for computing wave numbers dependent upon the PED. Table 2 shows the calculated spectral PED assignments, while Figures 2A,B show the theoretical FT-IR and FT-Raman spectrum.

C-H stretched wavelengths are typically seen in the 3100-3000 cm-1 region [29,30]. The compound affects the spectrum in the region, as mentioned above. Chemically aromatic CH stretch-ing of scaled frequencies is 98% over area 3095-2939 cm^{-1} through the greatest PED contribution. The FT-IR highly intense band theoretical bands were obtained at 3015-2900 cm^{-1}, while the FT-Raman high band spectrum was identified at 3005-2905 cm^{-1}.

A)

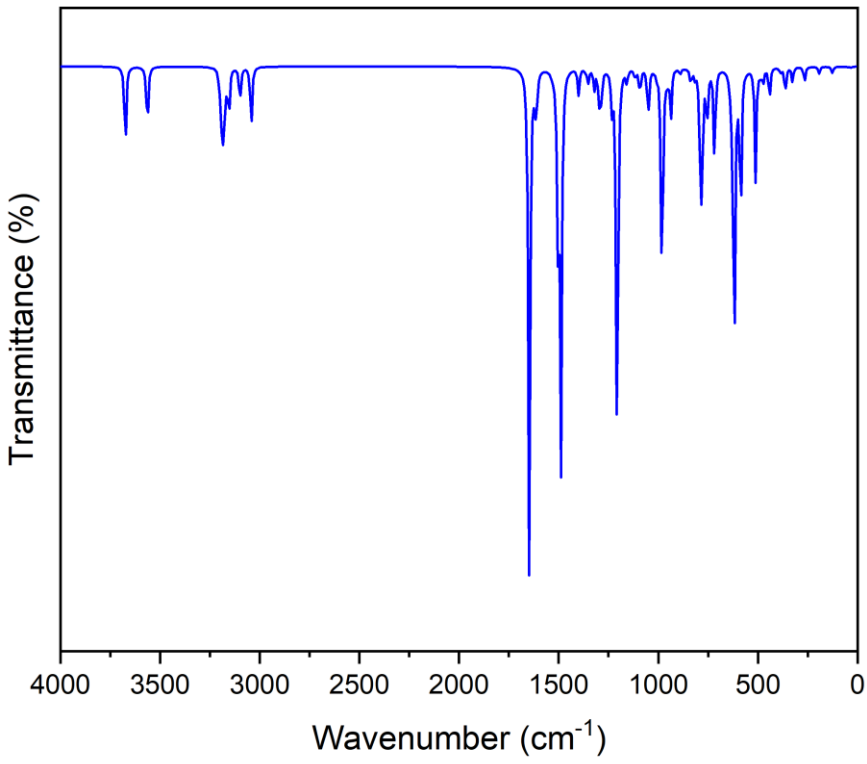

B

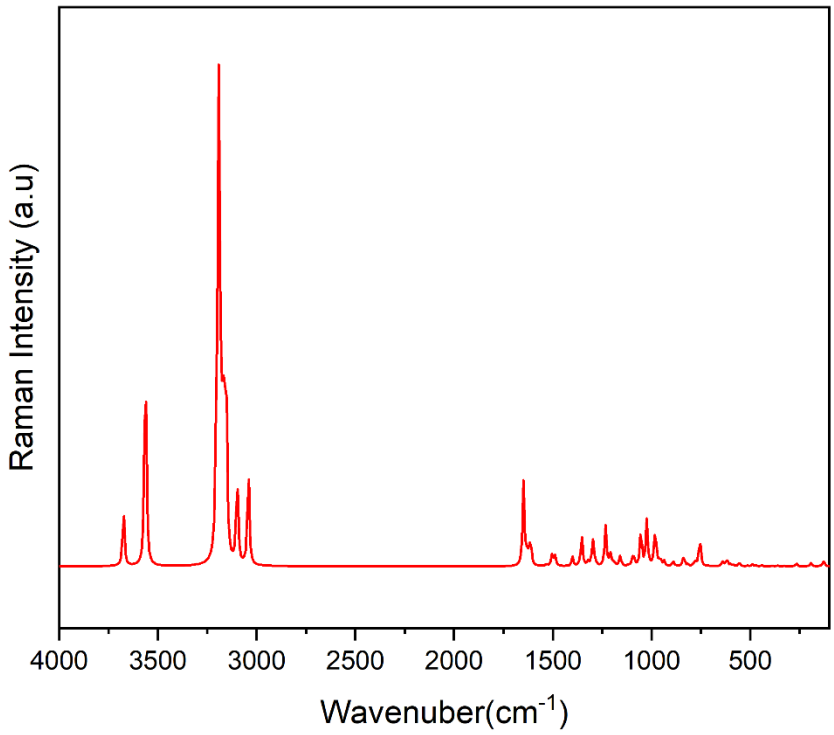

Figure 2. Theoretical FTIR and Raman spectra of 2-amino-3-benzyloxypyridine

C-C stretched wavelengths are typically seen in the 3100-3000 cm-^{1} region [31]. The theoretical predictions of the have been ascertained in the vicinity of 1588-488 cm-^{1} in C-C vibration. In FT-IR, the wavelengths were 1585, 1468, 1370, 1232, 1219, 1137, 1053, 953, 768, 758, 718, and 705 cm^{-1}. Raman peaks at 1500-598 cm^{-1} have been observed. The highest PED is 67%. C-N stretching bond vibrations have been observed to be recorded between 1561 and 1272 cm^{-1} [32]. It is quite challenging to discern C-N interactions in this spot due to the likelihood of vibration mingling. With 38% PED assignment, the C-N peaks in the title compound have been measured at 1437 cm-1 (IR) and 1238 cm^{-1}(Raman) theoretically**.** Carbonyl group frequently feature resonance structures, which affect compositional reactivity and enhance the groups level of polarity of the interaction [33]. The carbonyl C=O stretched mode has been estimated to be in the 1750-1600 cm^{-1}range [34]. C=O stretching vibration of evaluated scaled frequency at 1164- 937cm^{-1} in this work. The extremely strong band of C-O oscillations is detected in FT-IR at 1160 cm^{-1} and in FT-Raman (strong) at 930 cm-1. The impact of PEDs is 34%. NH vibration of stretching found solely in FT-IR at 3374 cm^{-1} occurs in a wideband in the current study. With PED 100%, the theoretically normalized frequency of NH vibration is 3552 cm-1. N-H stretching is the highest within the several vibrations of molecules [35], and the N-H bond's length is relatively short when compared to that of rest. As an outcome, this performs a function in an electrical shift.

Table 2. Calculated vibrational frequency with PED assignments with VEDA 4

S.no	Theoretical Wavenumber (cm^{-1})			PED
	Scaled	IR intensity	Raman activity	Assignments
1	3674	0	2	νNH (-49)+ νNH (50)
2	3563	0	2	νNH (50)+ νNH (49)
3	3202	0	1	νCH (55)+ νCH (43)
4	3190	1	1	νCH (-29)+ νCH (-22)+ νCH (-38)
5	3187	0	1	νCH (-44) + νCH (52)
6	3180	1	1	νCH (-11)+ νCH (14)+ νCH (-36)+ νCH (39)
7	3171	3	1	νCH (23) + νCH (-27) + νCH (42)
8	3163	3	0	νCH (-42) + νCH (33) + νCH (12) + νCH (-12)

9	3159	6	0	νCH (19) + νCH (21) + νCH (-18) + νCH (-23) + νCH (19)
10	3152	1	0	νCH (95)
11	3097	0	0	νCH (76)+ νCH (-24)
12	3041	6	0	νCH (24)+ νCH (76)
13	1644	3	0	νCC (30)
14	1643	1	1	νCC (26) + δHNH (30)
15	1625	22	0	νCC (-27) + νCC (20) +)+ δCCC (-10)
16	1615	0	1	νCC (27) + δHNH (22)
17	1607	32	0	νNC (13) + νCC (-11)+ νCC (11) + δHNH (21)
18	1527	2	0	δHCC (14)+ δHCC (16)+ δHCC (17)+ δHCC (18)
19	1499	67	2	δHCH (70)
20	1487	6	0	νNC (-12)+ δHCC (25)+ δHCN (13)
21	1484	0	1	δHCH (13)+ δHCC (18)
22	1483	20	0	νNC (12) + νNC (-12) + δHCN (-18)
23	1395	12	8	δHCO (-10)+ τHCOC (-27) + τHCOC (42)
24	1361	12	1	δHCO (11) + δHCC (-23)+ δHCC (23)+ δHCC (-10)+ δHCC (11)
25	1348	31	0	νNC (16) + νCC (10)+ δHNC (-13) + δHCN (29)
26	1343	2	0	νCC (18)+ νCC (15)+ νCC (-16)+ νCC (-13)+ δHCO (11)
27	1316	3	3	νNC (37)+ νNC (-16)+ δHCC (-10)
28	1292	0	0	νCC (-17)+ δHCC (22) + δHCN (10)
29	1280	1	1	δHCO (46)
30	1227	10	1	νCC (-39)+ δCCC (11)
31	1205	3	2	νOC (-10)+ δHCC (12)+ δHCC (15)+ δHCC (-12)+ δHCC (-11)
32	1200	13	4	νOC (23)+
33	1182	32	7	δHCC (-20)+ δHCC (18)+ δHCC (37)
34	1152	1	0	νCC (13)+ δHNC (-16)+ δHCC (-11)+ δHCC (38)
35	1111	1	0	νCC (-15)+ νCC (18)+ δHCC (13)+ δHCC (-13)
36	1086	0	0	νCC (16)+ νCC (32)+ δHCC (26)
37	1050	0	12	νCC (17)+ νCC (21)+ δCCC (-14)+ δHCC (11) + δHCC (11)
38	1045	10	4	νNC (17)+ νNC (10)+ νCC (11)+ δHNC (31)
39	1018	0	6	νCC (-13)+ νCC (-13)+ δCCC (-25)+ δCCC (-12)+ δCCC (18)
40	1005	6	4	τHCCC (20) + τHCCC (-13)+ τHCCC (-27)
41	1002	2	0	τHCOC (-15) + τHCOC (-15)
42	988	3	3	τHCCC (-18) + τHCCC (-19) + τHCCC (22)+ τHCCC (30)
43	978	0	1	νOC (34)+τHCCC (13) + τHCCN (-11)+ τHCNC (11)
44	970	64	2	νOC (34)+ τHCCN (-11)+ τHCNC (11)
45	950	24	2	τHCCC (51) + τHCNC (-20)
46	931	7	11	τHCCC (-26) + τHCCC (24)+ τHCCC (27)
47	884	7	1	νNC (16)+ δCNC (14)+ δNCC (-13)+ δCCC (27)
48	859	7	7	τHCCC (24) + τHCCC (26) + τHCCC (25)+ τHCCC (24)

49	831	4	1	νCC (15)+ δCCC (26)+ δOCC (-12)
50	810	1	0	τHCCN (29) + τCNCC (-14)+ τNCCC (11) + τCCCC (-14)
51	781	3	8	τHCCC (-15) + τHCCN (-31)+ τHCNC (-11) + OutNCNC (25)
52	771	0	0	δNCC (-10)+ τCCCC (11)
53	749	5	2	δNCC (19)
54	711	51	1	τHCCC (11) + τHCCC (-12) + τHCCC (16)+ τCCCC (11)+ τCCCC (33)+ τCCCC (-10)
55	635	21	1	δCCC (-25)+ δCCC (-10)+ δCCC (38)
56	628	13	1	δCOC (-10)+ δOCC (16)+ τCCCC (-10)
57	612	31	3	τHNCC (-24) + τHNCC (34)
58	595	1	0	δCCC (12)+ δOCC (-11)
59	580	8	6	δCNC (12)+ τHNCC (12)
60	549	4	3	δCCC (10)+ δCCC (11)+ OutNCNC (-12)
61	505	0	3	δCCC (-10)+ τCCCC (13))+ OutNCNC (18)
62	483	100	10	δCCO (-10)+ δNCN (15)+ OutCCCC (16)
63	468	0	12	δCCO (15)+ δNCN (-14)+ τHNCC (15)+ τHNCC (10)
64	435	13	28	δCCO (12)+ τHNCC (-31)+ τHNCC (-26)
65	413	8	26	τHCCC (11)+ τHCCC (12)+ τCCCC (-35)+ τCCCC (13)+ τCCCC (-20)
66	380	8	40	δCOC (12)+ τCCCC (-10)+ τCCCC (14)
67	356	1	4	δCCC (-32)+ τHCOC (11)
68	319	0	29	δCCO (14)+ δNCN (14)+ δCCC (32)
69	259	4	31	τCCCO (-13)
70	185	12	11	δCOC (12)+ τNCCC (-39)+ τCCCC (10)
71	124	6	25	δOCC (-11)+ τCCCO (-20)+ OutCCCC (24)
72	119	6	100	δCOC (-16)+ δCCC (-10)+ δOCC (-11)+ τCCCO (24)
73	41	3	44	τCCOC (42)+ τCOCC (-23)+ OutCCCC (-13)
74	30	14	65	τOCCC (82)
75	24	17	16	τCCOC (-34)+ τCOCC (-46)

a) Scaling factor: 0.96 above 3000 cm−1 and 0.961 below 3000 cm−1 for B3LYP/6- 311++G(d,p).
b) Relative absorption intensities normalized with highest peak absorption equal to 100.
c) Relative Raman intensities normalized to 100.
d) ν- Stretching, β- bending, ω – out of plane, τ-torsion.

3.3. HOMO LUMO Analysis

Gaussian program has been implemented to calculate the FMO investigation [36]. The terms "HOMO" and "LUMO" refer to the e- receiver and contributor [37]. These orbital structures, which form and are attached to the compound and permit the strongest interaction, are also known as frontier orbitals [38]. The B3LYP basis set has been employed to figure out the HOMO-LUMO difference in energy (energy gap (Eg)), which elucidates the transmission of charge exchanges among 2A3BP. A schematic representation Figure 3 illustrates the disparity in energy for a variety of solvents. HOMO-LUMO separation of energy for 2A3BP is 5.164 eV. Energy gaps demonstrate the substance's bio-activity in nature. High stability indicates less chemical reactive properties, while inadequate stability implies significant reactivity to chemicals [39]. Large energy gaps suggest that a compound is very stable, while tiny energy gaps indicate that a compound is poorly stable. Increasing the softness number broadly, the hardness level and chemical reactivity ought to be increased [40]. Amino benzyl is the location of HOMO, while benzyloxy pyridine is the location of LUMO.

Energy Band Gap(ΔE) = DMF=DMSO =Gas= CH3OH=Water › C2H6O › Chloroform

Ionization Energy(IP) = Gas=Water› DMSO›DMF›CH3OH›C2H6O›Chloroform

Electron Affinity(EA) = Gas = Water › DMSO › DMF › CH3OH › C2H6O › Chloroform

Electronegativity(χ) = Gas = Water › DMSO › DMF ›CH3OH› Ethanol ›Chloroform

Chemical potential (μ) = Chloroform› C2H6O › CH3OH › DMF › DMSO › Gas = Water

Chemical hardness (η) = DMSO = DMF = Gas = CH3OH = Water › C2H6O› Chloroform

Softness (ς) = Chloroform› Gas = DMF = DMSO = C2H6O = CH3OH = Water

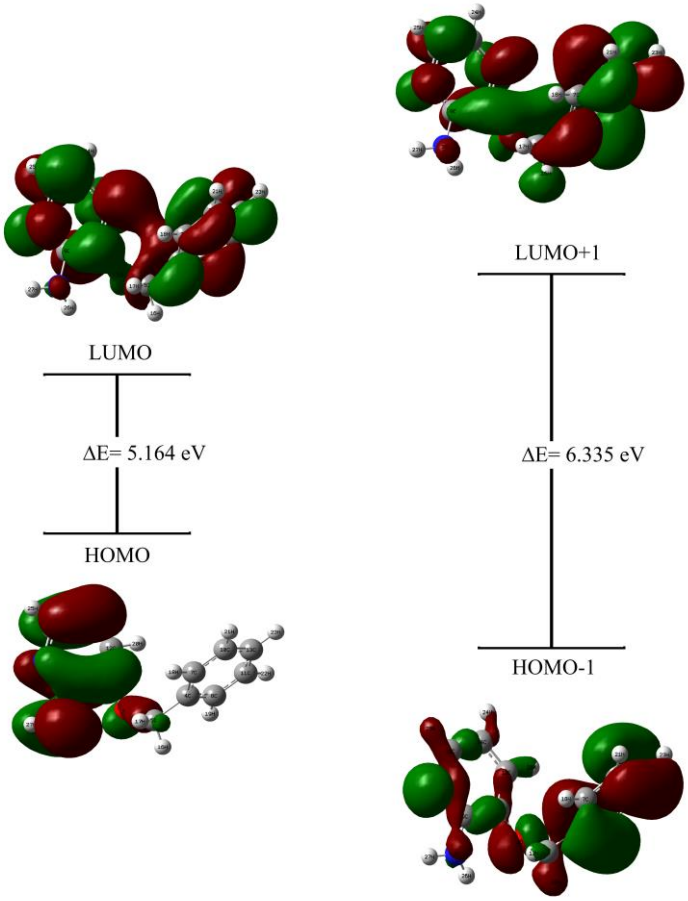

Figure 3. MOs orbital of 2-amino-3-benzyloxypyridine

Parameters	**Values (eV)**									
	Medium									
	Gas	**Water**	**Methanol**	**Ethanol**	**Chloroform**	**DMSO**	**DMF**	**Benzonitrile**	**Benzylalcohol**	**TFE**
E_{HOMO}	-6.2015	-6.2015	-6.1955	-6.1922	-6.1422	-6.1985	-6.1969	-6.1925	-6.1794	-6.1930
E_{LUMO}	-1.0373	-1.0373	-1.0313	-1.0283	-0.9856	-1.0343	-1.0327	-1.0286	-1.0163	-1.0291
Energy Band Gap (ΔE	5.1642	5.1642	5.1642	5.1639	5.1566	5.1642	5.1642	5.1639	5.1631	5.1639
Ionization energy (IP	6.2015	6.2015	6.1955	6.1922	6.1422	6.1985	6.1969	6.1925	6.1794	6.1930
Electron affinity (EA	1.0373	1.0373	1.0313	1.0283	0.9856	1.0343	1.0327	1.0286	1.0163	1.0291
Electronegativity(χ)	3.6194	3.6194	3.6134	3.6103	3.5639	3.6164	3.6148	3.6105	3.5979	3.6111
Chemical potential (μ	-3.6194	-3.6194	-3.6134	-3.6103	-3.5639	-3.6164	-3.6148	-3.6105	-3.5979	-3.6111
Chemical hardness (η)	2.5821	2.5821	2.5821	2.5820	2.5783	2.5821	2.5821	2.5820	2.5815	2.5820
Softness (ς)	0.3873	0.3873	0.3873	0.3873	0.3879	0.3873	0.3873	0.3873	0.3874	0.3873
Electrophilicity inde (ω)	2.5367	2.5367	2.5283	2.5241	2.4631	2.5325	2.5302	2.5245	2.5072	2.5252
Maximum charge transfer index (ΔNmax)	1.4017	1.4017	1.3994	1.3983	1.3823	1.4006	1.3999	1.3984	1.3937	1.3986
Optical Softness ($\sigma_\circ$)	0.1936	0.1936	0.1936	0.1937	0.1939	0.1936	0.1936	0.1937	0.1937	0.1937

Nucleophilic index (N)	0.3942	0.3942	0.3955	0.3962	0.4060	0.3949	0.3952	0.3961	0.3989	0.3960

3.4. UV Analysis

Both static and dynamic properties, along with the electronic changes, are examined using UV-Vis spectroscopy. DFT approach and (IEFPCM) method are used to get the theoretical spectrum of using the Gas and various solvent phases [41]. According to the greatest band-gap, valance--electrons nearly the nucleus on the ring is predicted [42,43]. UV-Vis spectra are depicted in Figure 4. Table 4 contains information contribution. An absorption spike in the gas phase at 274 nm corresponds to a maximal peak value. This compound's band gap is Others, such as Methanol, Water, Gas, Ethanol, DMSO, DMF, Chloroform, Benzonitrile, Benzyl alcohol and TFE have the longest wavelengths of 273.97, 274.12, 274.14,274.14, 274.24, 274.44, 274.48, 274.68, 274.79, 274.81, 274.97 nm respectively.

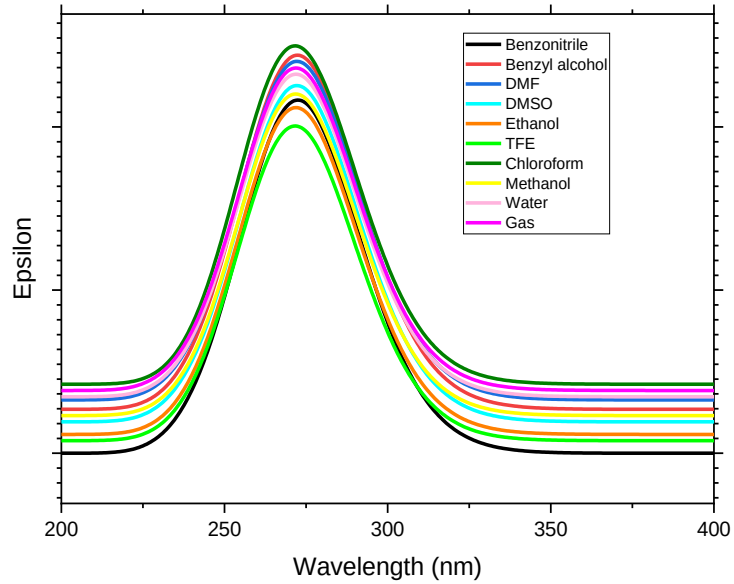

Figure 4. UV-Vis spectra of 2-amino-3-benzyloxypyridine

Table 4. Absorbance parameters of 2-amino-3-benzyloxypyridine

Solvents	λ_{max} (nm)	ΔE (eV)	Oscillator strength (f)	Major contribution (%)
Gas	274.14	4.5226	0.1120	HOMO->LUMO (95%)
Water	274.14	4.5226	0.1120	HOMO->LUMO (95%)
Methanol	274.12	4.5230	0.1109	HOMO->LUMO (95%)
Ethanol	274.24	4.5211	0.1125	HOMO->LUMO (95%)
Chloroform	274.68	4.5138	0.1085	HOMO->LUMO (95%)
DMSO	274.44	4.5177	0.1168	HOMO->LUMO (95%)
DMF	274.48	4.5170	0.1174	HOMO->LUMO (95%)
Benzonitrile	274.79	4.5120	0.1224	HOMO->LUMO (95%)
Benzylalcohol	274.81	4.5116	0.1209	HOMO->LUMO (95%)
TFE	273.97	4.5255	0.1081	HOMO->LUMO (95%)

3.5.MEP and ALIE Analysis

MEP investigation has been determined using various hues on the MEP mapping representing distinct

electrostatic potentials [44,45]. It also makes it possible for us to determine the substance's dimensions, form, and density of electrons[46]. The most -Ve electrostatic potential is displayed in the red color zone, the highest +Ve electrostatic potential was represented in the blue color zone, and zero potential was indicated in the green region[47]. MEP plot is depicted in Figure 5 for gas and for the solvent phase. The colors red and blue symbolize the most potent attraction and repulsion, respectively. The -ve potential area is typically linked with loan pair electronegative atoms. The molecule with the blue zone (positive potential) is positioned at all hydrogen atoms and the H-CH group, which is more attractive, and the reddish area (negative potential) is located at the N = C = N group, which is the more reactive site.

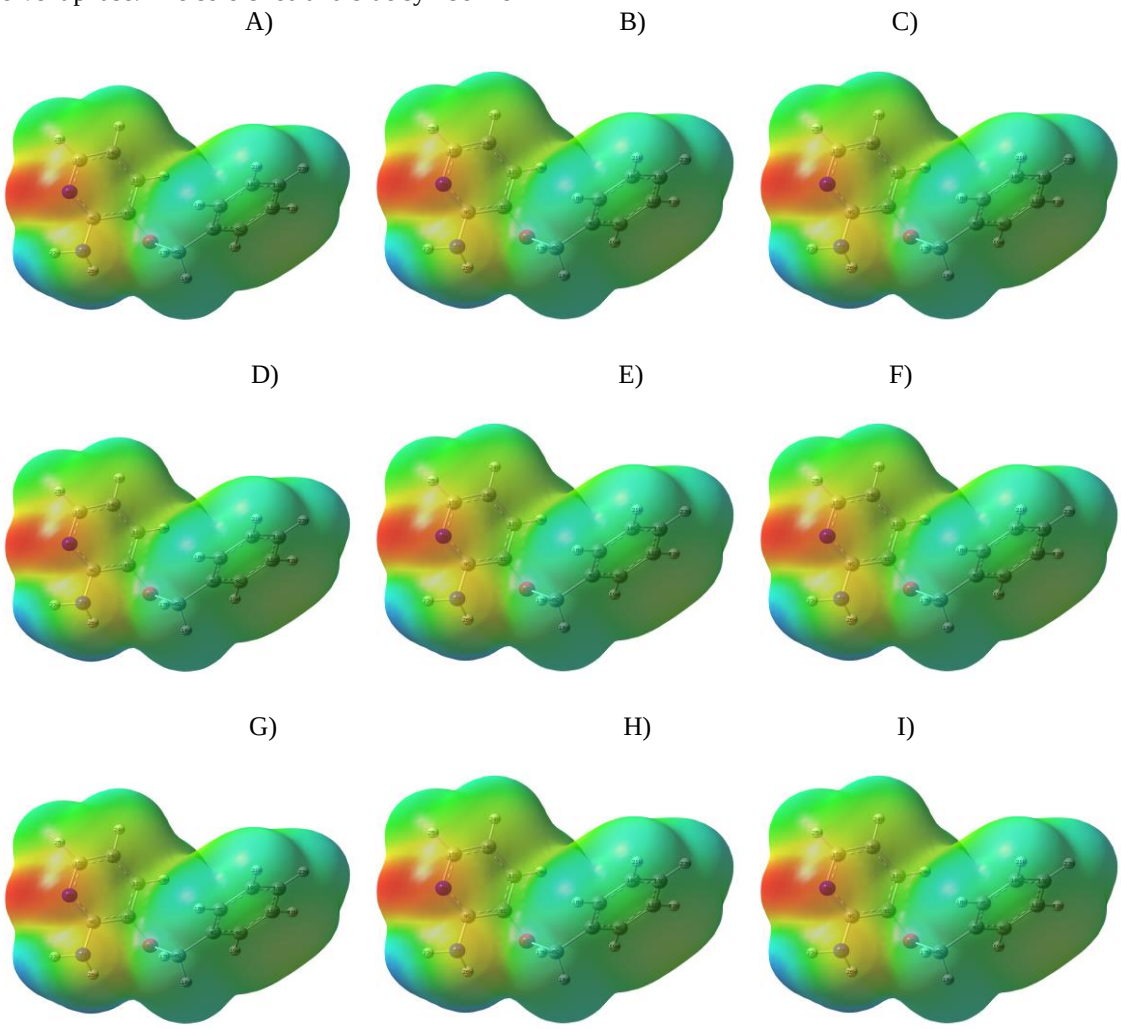

Figure 5. MEP and ESP surfaces of 2-amino-3-benzyloxypyridine in solvent A) water, B) methanol, C) ethanol, D) chloroform, E) DMSO, F) DMF, G) benzonitrile, H) benzylalcohol, and I) Gas

ALIE investigation delivers evidence approximately for a material's localized interaction. When a charged particle gets ejected from the site of the structure, it may be accurately identified [80]. ALIE plot is depicted in Figure 5A for the gas phase and solvent. The sigma (σ) bond in the molecular structure promotes an effective interaction between atoms, promoting stability. The presence of the blue hue, which corresponds to nitrogen atoms, indicates that those spots are inclined to receive protons. “Red Zone” refers to the area between 1.500 to 2.30, signifies a concentrated presence of atoms with a positive charge, specifically located in the interior electron shells of heavier elements such as carbon (C) and hydrogen (H).

A) B) C)

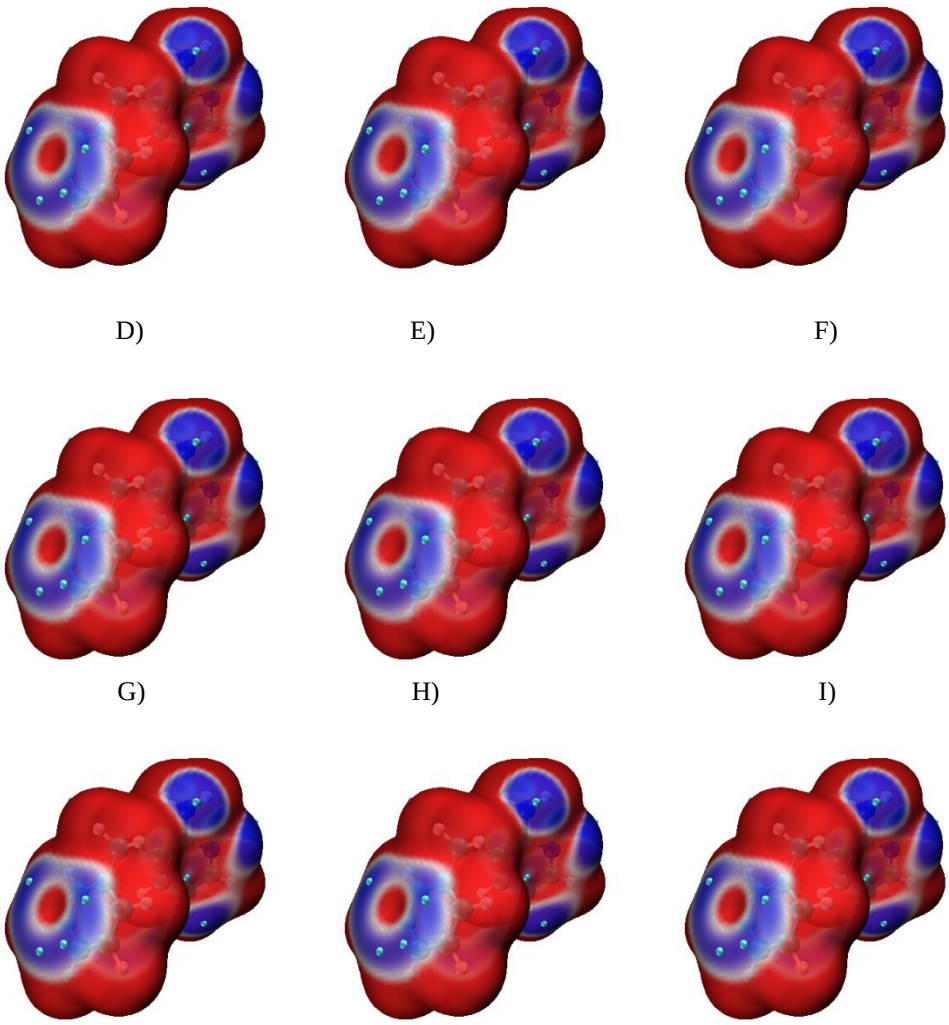

Figure 5A. ALIE surfaces of 2-amino-3-benzyloxypyridine in solvent A) water, B) methanol, C) ethanol, D) chloroform, E) DMSO, F) DMF, G) benzonitrile, H) benzylalcohol, and I) Gas

3.6. NBO Analysis

Evaluating conjugative connections or the transfer of charge in systems of molecules can be done with the help of natural bond orbital analysis[48]. It determines the energies of bonding, anti-bonding, and donor-acceptor delocalization[49]. Larger conju-gation is indicated by high E(2) value. De-localization of electron numbers in Lewis and non-Lewis NBO orbitals[50], which is associated with stabilizing acceptor-donor interactions. Similar to how the primary hybrid-conjugative relationship overlaps with π- σ*, the second conjugative interaction does the same for n- π*, n- r*, and π- π* orbitals[51-52]. Table 5 contains information on NBO analysis. The LP1O1, LP2O1, LP1N2, and LP(1)N3 to anti-bonding σ*(C6-C9), σ*(C4-C5), σ*(C6-C9), π*(N2-C9), and π*(S29-O30) have the highest stabilisation energies, which were measured at 3.20, 5.93, 10.87, 33.24. Furthermore, the highest stabilisation energy is 20.18, 15.13, 20.33 and 23.78 kcal/mol, due to the bonding C4-C7, C6-C12, C10-C13 and C14-C15 to anti- bonding π*(C10-C13), π*(C14-C15), π*(C4-C7) and π*(C6-C12), with occupancy is 1.65809,1.70633, 1.66628 and 1.69053 respectively; and bonding C4-C7 and C8-C11 to anti-bonding π*(C7-C10) and σ*(C11-H22) with occupancy is 1.97333 and 1.97769.

Table 5. Second order perturbation theory analysis of fock matrix in NBO basis

Donar	Occupancy	Acceptor NBO (j)	ED	E(2) kcal/mol	E(j)-E(i) a.u.	F(i,j) a.u.
$\sigma(O_1\text{-}C_5)$	1.97483	$\pi^*(C_6\text{-}C_{12})$	0.02764	2.57	0.81	0.044
$\sigma(N_2\text{-}C_9)$	1.98148	$\sigma^*(C_6\text{-}C_9)$	0.05172	2.94	1.75	0.057
$\pi(N_2\text{-}C_9)$	1.71827	$\pi^*(C_6\text{-}C_{12})$	0.32755	11.23	0.33	0.055
$\pi(N_2\text{-}C_9)$	1.71827	$\pi^*(C_{14}\text{-}C_{15})$	0.31495	27.62	0.33	0.086
$\sigma(N_3\text{-}C_9)$	1.98901	$\sigma^*(N_2\text{-}C_{15})$	0.01321	2.60	1.36	0.053

$\sigma(C_4- C_7)$	1.97333	$\sigma^*(C_4-C_8)$	0.02627	4.13	1.27	0.065
$\sigma(C_4- C_7)$	1.97333	$\sigma^*(C_7- C_{10})$	0.01639	3.44	1.27	0.059
$\pi(C_4-C_7)$	1.65809	$\pi^*(C_8-C_{11})$	0.31377	20.29	0.28	0.068
$\pi(C_4-C_7)$	1.65809	$\pi^*(C_{10}-C_{13})$	0.32277	20.18	0.28	0.068
$\pi(C_6- C_{12})$	1.70633	$\pi^*(N_2-C_9)$	0.44677	26.69	0.28	0.080
$\pi(C_6- C_{12})$	1.70633	$\pi^*(C_{14}-C_{15})$	0.31495	15.13	0.30	0.060
$\sigma(C_7- H_{18})$	1.97942	$\sigma^*(C_4-C_8)$	0.02627	4.62	1.09	0.063
$\sigma(C_8- C_{11})$	1.97769	$\sigma^*(C_{11}-H_{22})$	0.01460	1.15	1.14	0.032
$\pi(C_{10}- C_{13})$	1.66628	$\pi^*(C_4-C_7)$	0.34546	20.33	0.29	0.069
$\pi(C_{10}- C_{13})$	1.66628	$\pi^*(C_8-C_{11})$	0.31377	19.92	0.28	0.068
$\sigma(C_{11}- H_{22})$	1.97964	$\sigma^*(C_4-C_8)$	0.02627	4.04	1.09	0.059
$\pi(C_{14}- C_{15})$	1.69053	$\pi^*(N_2-C_9)$	0.44677	13.73	0.27	0.056
$\pi(C_{14}- C_{15})$	1.69053	$\pi^*(C_6-C_{12})$	0.32755	23.78	0.28	0.074
LP1O1	1.94566	$\sigma^*(C_6-C_9)$	0.05172	3.20	1.06	0.052
LP2O1	1.92675	$\sigma^*(C_4-C_5)$	0.03189	5.93	0.76	0.060
LP1N2	1.90748	$\sigma^*(C_6-C_9)$	0.05172	10.87	0.86	0.087
LP1N2	1.90748	$\sigma^*(C_{14}-C_{15})$	0.02522	8.83	0.91	0.081
LP1N2	1.90748	$\sigma^*(C_{15}-H_{25})$	0.02437	4.27	0.77	0.52
LP1N3	1.82099	$\pi^*(N_2-C_9)$	0.44677	33.24	0.31	0.97
$\pi(N_2- C_9)$	1.71827	$\pi^*(C_6-C_{12})$	0.32755	198.40	0.02	0.085
$\pi(N_2-C_9)$	1.71827	$\pi^*(C_{14}-C_{15})$	0.31495	141.78	0.02	0.078
$\pi(C_4- C_7)$	0.34546	$\sigma^*(O_1-C_5)$	0.03762	3.31	0.23	0.056
$\pi(C_6- C_{12})$	0.32755	$\sigma^*(O_1-C_5)$	0.03762	1.17	0.23	0.034

a E2 means energy of hyper conjugative interaction (stabilization energy).
b E(j)-E(i) is the energy difference between donor i and acceptor j.
c F(i,j) is the Fock matrix element between i and j NBO orbital's.

3.7. Mulliken Charge Analysis

Mulliken distribution[53] of charges for 2A3BP is computed at the same basic level as above. Figure. 6 depicts a visual illustration of the distribution. There are twenty-four atoms in2A3BP, and each one has a significant charge. The greatest +ve charge is a carbon (C4). Next priority H27 has +ve charge (0.754282) by reason of the localization of extra electro-negative oxygen(O) atoms. Hydrogen atoms received the next highest priority positive charge since they are attached to carbon atoms also there are no electrons present, all those hydrogen elements in ring exhibit +ve charges on them. Oxygen (O1), nitrogen (N1, N2), and all the carbon atoms (C4-C15) had negative charges. Negative charges have been detected in both of the O2 atoms, with the highest negative charge at C9 (-0.11926).

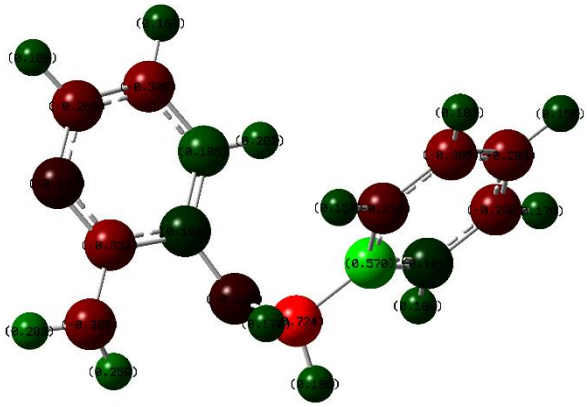

Figure 6. Muliken charge distribution of 2-amino-3-benzyloxypyridine

3.8. TDOS Analysis

Gauss sum technique was used to project the density of electrons along with additional probable solvent sites; the plots are shown in Figure 7. In the DOS spectrum [54], green and blue streaks represent HOMO and LUMO states. According to DOS, energy gap Eg =5.164 eV for gas and a solvent energy gap of eV for water, which is almost the same. DE H-L and DE DOS energy discrepancies roughly match these results. In gas and solvent state, the DOS spectrum reveals a high concentration of e- at HOMO and a tiny amount of e- closer to the LUMO. This implies that there's a potential for the e-cloud to split over occupied and reinstate with LUMO. According to DOS investigations, e-cloud which may be used to activate the electron(e-) conversion. Therefore, it is manifest that the solvent inflates the spectral gap(Eg).

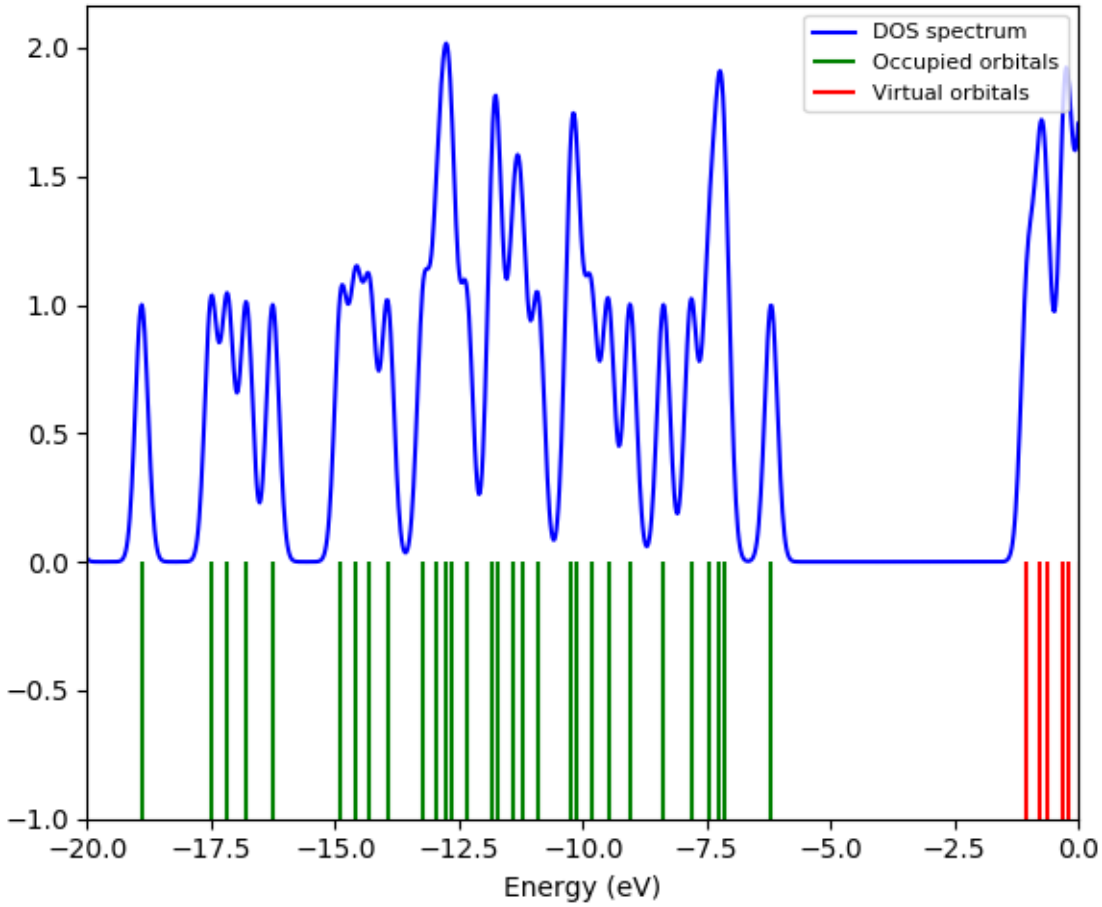

Figure 7. DOS Plot for gas phase

3.9. Thermodynamic Properties

The progression and kinetic coherence of a substance's reactions are predicted using thermochemical calculations [55]. Gibbs-free energy and enthalpy measure energy release and consumption, which influence the formation of bonds [56]. Significant numbers imply that there are more binding sites, whereas low values suggest impulsive binding. Compounds without external energy for binding have -ve free energy and enthalpy values. Table 6 shows the values.

Zero-point correction**:** DMF›Gas›Ethanol›Water›DMSO=Methanol

Energy: Methanol › DMSO › Ethanol › DMF › Gas › Water

Enthalpy: Methanol › DMF › Ethanol = DMSO › Gas =Water

Gibbs Free Energy: Ethanol = Methanol › DMSO › Gas › DMF › Water

Zero Point Energies: Ethanol › Methanol = Water › DMF › DMSO › Gas

Electronic and Thermal Energies: Water › Ethanol › Gas = Methanol › DMF › DMSO

Electronic and Thermal Enthalpies: Water › Methanol › DMSO › DMF › Ethanol › Gas

Sum of Electronic and Thermal free Energies: Water › DMSO › Gas › DMF › Ethanol › Methanol

Table 6. Thermodynamic properties of 2-amino-3-benzyloxypyridinefor the gas and solvent phase

	Gas	DMF	**DMSO**	**Water**	**Ethanol**	**Methanol**
Zero-point correction	0.218618	0.218718	0.218118	0.218218	0.218418	0.218118
Energy	0.231114	0.231214	0.231414	0.231014	0.231314	0.231914
Enthalpy	0.232058	0.232258	0.232158	0.232058	0.232158	0.232958
Gibbs Free Energy	0.177613	0.177113	0.177713	0.177013	0.177913	0.177913
zero-point Energies	-649.1812	-649.1412	-649.1612	-649.1112	-649.1112	-649.1112
Electronic and thermal Energies	-649.1687	-649.1787	-649.1887	-649.1287	-649.1587	-649.1687
Electronic and thermal Enthalpies	-649.1677	-649.1477	-649.1277	-649.1077	-649.1577	-649.1177
Sum of electronic and thermal Free Energies	-649.2222	-649.2322	-649.2122	-649.2022	-649.2522	-649.2922

3.10 TDM Analysis

TDMs (Transition Density Matrix) [57] tell the disparities between the ground and prominent (simulated) phases of a molecule. TDMs also display the proposed structural shapeshift. The sites of the unit that was donated and the receiver might be shown using TDM maps in Figure 8. The excitement Energy for E2=3.038eV, E3=3.276eV, and E1=2.657eV. Hydrogen atoms are grooved in a crook during excitation, and TDMs provide better consequences. Overall, each component in the structure of a molecule was impacted, although hydrogen only made a small contribution; thus, it wasn't included in the analysis.

A) S0 Excitation **B) S1 Excitation**

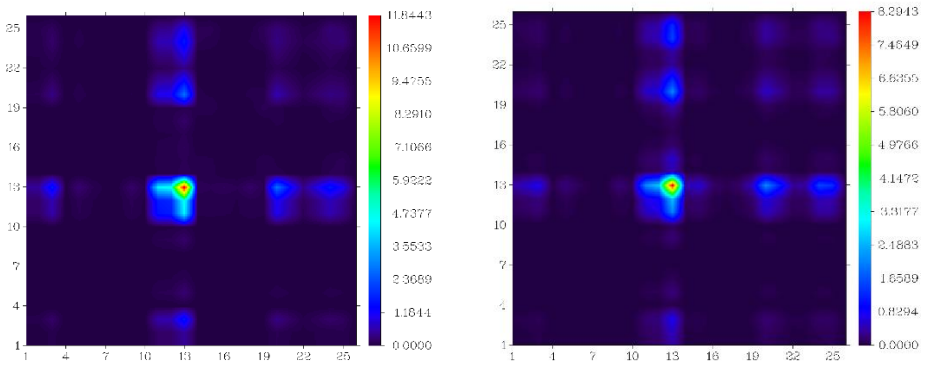

C) S2 Excitation

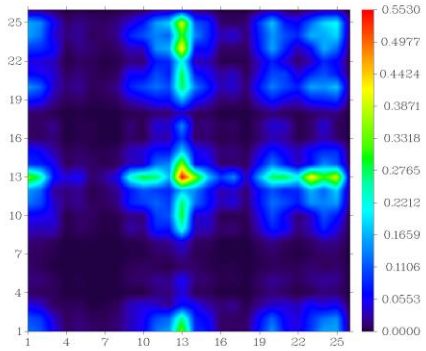

Figure 8. TDM's over the material of 2-amino-3-benzyloxypyridine for three excited states in gas phase

3.11. Topology-Analysis

3.11.1.ELF and LOL

LOL and ELF are identically primary studies for understanding topological analysis[58,59]. LOL refers to intense, confined orbital overlay, while ELF signifies the number of pairs of electrons per area unit defined by orbital gradient [60]. Figure 9(A,B) and depict the topological mappings for ELF & LOL in the gas phase. Blue to red are the primary hues. The value for ELF ranges from 0.000 to 1.000, whereas the value range for

LOL ranges from 0.000 to 0.800. A colour range of less than 0.5 indicates the region is de-localized, whereas a colour range of more than 0.5 suggests the region zone is localised. The hue a light blue indicates the inner shell's electron reductions and valence. Due of stronger Pauli repulsion, H21 and C16 dominate electron localisation. The electron de-localization orbitals shown in blue. A substantial LOL value over the covalent region suggests the presence of a red color. In LOL, an inner section of an H-atom emerges white because its density of electrons surpasses the top limit. A blue circle represents the location of particle loss through the valence to the inner shelve.

A)

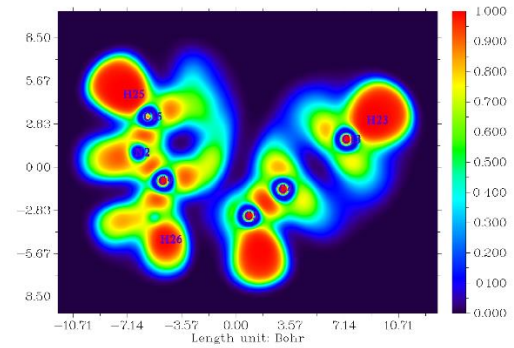

B)

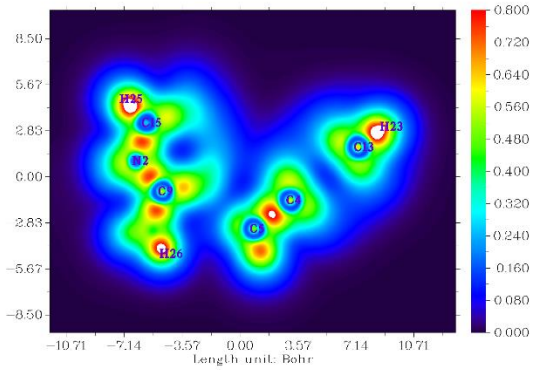

Figure 9(A,B) ELF and LOL maps of 2-amino-3-benzyloxypyridine in the gas phase

3.11.2. IRI and RDG

In molecular structures, inter-atomic interactions are frequently seen. Because IRI may identify thinner interacting regions in molecules, It is extremely valuable in the research of diverse molecular configurations and biochemical processes[61]. IRI is reliant on electron density and is useful for identifying chemical interactions in bio-molecules [62]. In Figure 10 blue iso-surfaces denote an area through an elevated density of electrons that strengthens the connection between the molecules, green iso-surfaces depict a weak-connection zone, and red iso-surfaces depict the act of steric or repulsive forces [63].

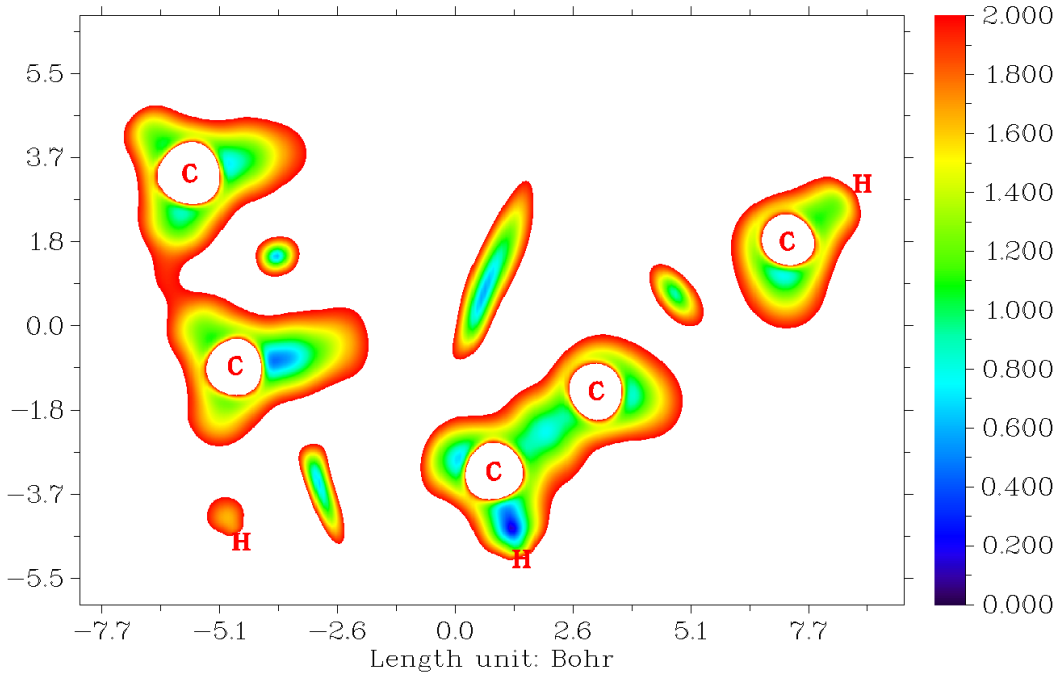

Figure 10. IRI surface plot of 2-amino-3-benzyloxypyridine in gas phase

NCI provides a thorough examination of attractive (bond-ing) & repulsive (non-bonding) interactions inside a study molecule, providing complete information on these areas [64]. This method inspects non-covalent connections [65] between intra and intermolecular substances [66] based on electron density and metabolites. Figure 11(I, II) depicts the gradient (RDG) vs electron density. The enhanced favorable interactions in the blue-spotted area of the RDG scatter plot are ascribed to robust hydrogen bonds. The vibrant red hue of the ring accentuates the steric impact occurring within a region of favorable dispersion. Van der Waals interactions are observable in the RDG plot and can be distinguished in areas that appear green.

A)

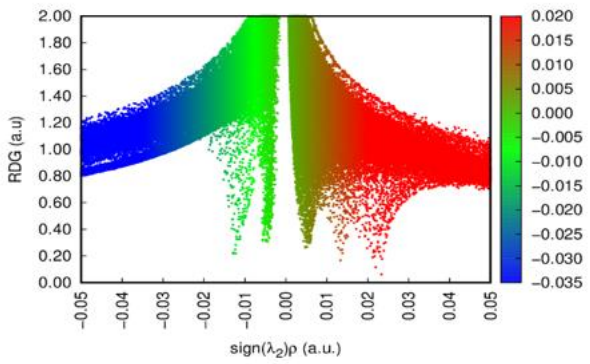

B)

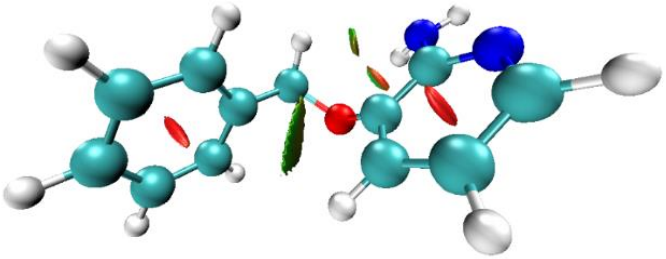

Figure 11(A,B) RDG Plots versus the electron density ρ multiplied by the sign of λ2 for gas phase ,2D scatter and Isosurface density plots illustrating the non-bonded interactions of 2-amino-3-benzyloxypyridine in gas phase

3.12 Pharmacological Properties

3.12.1 Biological Aspects

Pharmaceutical function refers to the beneficial impact of drugs on living organisms [67]. A pharmaceutical product is a chemical that links to biological substances. Bio-targets include receptors for antibodies, enzymes, amino acids, and ion channels [68]. The word "drug target" can also refer to a biological target. All variables were determined via the internet. The biological function of the title chemical was calculated utilizing molinspiration.

The biological activities score of an organic compound is classified according to its degree of biological activity. An active compound is defined as having a score above zero. If the value is within the range of 0 to 5, it is considered moderately active and advantageous. Conversely, if the number is below 5, it is seen as ineffectual [68]. The molecule in issue has significant activity, with a GPCR-ligand activity of 0.04, demonstrating its level of activity. The ICM value is 0.14, which also signifies activity. A KI value of 0.07 indicates that it is actively functioning, whereas an NRL value of 0.23 denotes that it is moderately active. The chemical is considered active based on its PI and EI values, which are 0.03 and 0.23, respectively [69,70]. Table 7 summarises the predicted bioactivity score of the title chemical. This demonstrates that the molecule contains the properties required for it to be a medicine.

Table 7. Bioactivity score prediction of 2-amino-3-benzyloxypyridine

Bioactivity score prediction	
GPCR ligand	-0.18
Ion channel modulator	-0.67
Kinase inhibitor	-0.37
Nuclear receptor ligand	-2.08
Protease inhibitor	-0.31
Enzyme inhibitor	-0.69

>0 = active, -5.0-0.0 = moderately active, <-5.0= inactive

3.12.2 Drug Likness Activity

Drug similarity is a concept used in therapeutic progress [71]. The issue is described as the natural state of a compound's bio-cellular properties, the influence of its pharmaceutical subtleties, pharmaceutical kinetic, and ADMET in the body of a person [72]. Multiple guidelines have been presented for determining drug-likeness. Veber rules [73] , and Lipinski's rule of five [74] are the ones most frequently used & have been shown to be exceptionally efficacious and cost affordable. These are intended to be fundamental principles rather than definite rules for determining whether a perhaps the component is drug-like nor not. Table 8 and Table 9 summarizes the calculated requirements and compare them to Lipinski's results and ABMET fallouts. The overwhelming mainstream of compounds have log p values(<5), (<10)HBA, HBD=(5), a MM (>500 Daltons), and RB(<10), according to the rule. Based on the data pointed out above, the molecule BBT has been developed so it has the expected pharmacokinetics sensors and boiled-Egg image for the BBT. Figure 12 shows that BBT is prominent on the biological absorption radar. (BOILEDEGG[75] is an efficient and important approach for the creation of drugs. When given orally, an active medicine frequently violates the criteria just once. These data show that (ligand's) oral bioavailability is satisfactory and that it satisfies the stipulated standards.

Table 8 Drug likeness and liphophilicity parameters of 2-amino-3-benzyloxypyridine

Descriptors	**Values**	**Fall within optimum range (Yes/No)**
Hydrogen bond donor (HBD)	0	Yes
Hydrogen bond acceptor (HBA)	2	Yes
AlogP	3.537	Yes
Polar surface area (TPSA) [Å2]	55.26	Yes
Number of rings	2	Yes
Number of heterocyclic atoms	12	Yes
Molecular weight	257.35	Yes
Molar refractivity	75.61	Yes
Number of heavy atoms	18	Yes
Number of rotatable bonds	4	Yes
Formal charge	0	Yes
Lipophilicity details		
XLOGP	3.04	
WLOGP	3.54	
MLOGP	2.47	
Silicos-IT Log p	4.28	
iLOGP	2.54	
Consensus LogP	3.17	

Table 9. ADMET properties of 2-amino-3-benzyloxypyridine

Property	**Model Name**	**Predicted Value**	**Fall within optimum range (Yes/No)**
Absorption	water solubility	-3.158	Yes
Absorption	Caco2 permeability	1.256	Yes
Absorption	Intestinal absorpion(human)	94.903	Yes
Absorption	Skin permeability	-2.88	Yes
Absorption	P-glyoprotein substrate	No	Yes
Absorption	P-glyoprotein I inhibitor	No	Yes
Absorption	P-glycoprotein II inhibitor	No	No
Distribution	VDss(human)	0.322	No
Distribution	Fration unbound (human)	0.365	Yes
Distribution	BBB permeability	0.478	No
Distribution	CNS permeability	-2.014	No
Metabolism	CYP2D6 substrate	No	-
Metabolism	CYP3A4 substrate	No	-
Metabolism	CYP1A2 inhibitor	Yes	-
Metabolism	CYP2C19 inhibitor	No	-
Metabolism	CYP2C9 inhibitor	No	-
Metabolism	CYP2D6 inhibitor	No	-
Metabolism	CYP3A4 inhibitor	No	
Excretion	Total Clearance	0.53	Yes
Excretion	Renal OCT2 substrate	No	Yes
Toxicity	AMES toxicity	No	No
Toxicity	Max. tolerated dose(human)	0.311	No
Toxicity	hERG I inhibitor	No	No
Toxicity	hERG II inhibitor	No	No
Toxicity	Oral Rat Acute Toxiity(LD50)	2.775	No
Toxicity	Oral Rat Chronic Toxicity(LD50)	1.796	No
Toxicity	Hepatotoxicity	Yes	Yes
Toxicity	Skin Sensitisation	No	Yes
Toxicity	T.Pyriformis toxicity	0.307	-
Toxicity	Minnow toxicity	2.162	-

A)

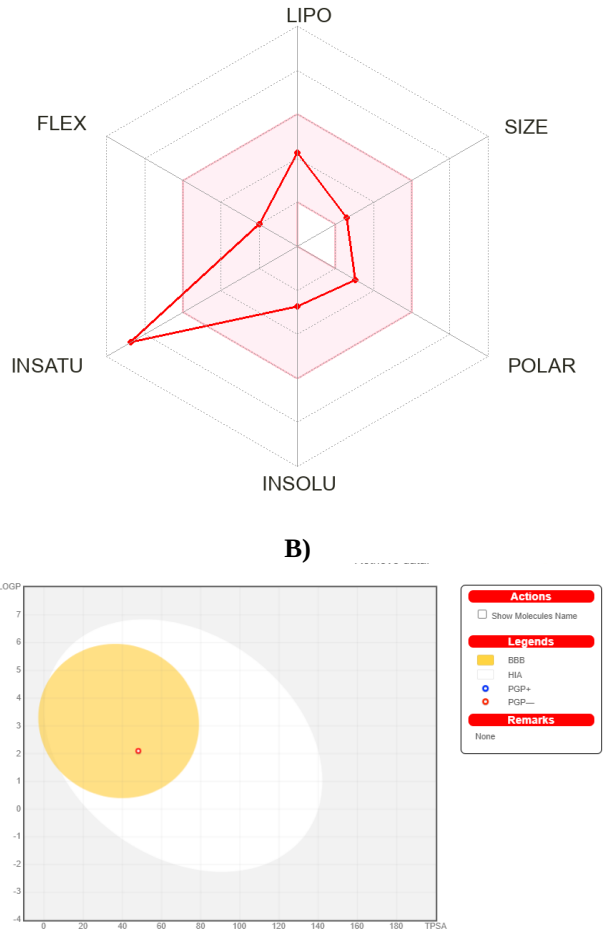

Figure 12 A) Bioactivity radar B) Predicted Boiled egg plot of 2-amino-3-benzyloxypyridine

3.12.3 Molecular Docking

Molecular docking has progressed as a popular implement for studying the connection amid structure-activity interactions and medication innovation [76]. Using the program PASS online[77], the title compound's optimized structure in SMILES setup was used to forecast its biotic activity. This method has a reputation for producing very precise results. It is feasible to regulate the binding energy and position of the ligand and macromolecules [78]. RCSBs protein data bank Wesbite [79] was used to generate the target proteins for anti-viral (5XUI and 4IIT). This docking research has been carried out utilizing the Auto Dock programs, it can determine the optimal binding location for interactions among proteins and ligands. Proteins (5XUI and 4IIT) responded strongly because of docking, with BE of (-9.10 and -6.18 kcal/mol). (PDB-5XUI) including the drug has the highest BV (-9.10 kcal/mol) as well as numerous interactions. For 4IIT two hydrogen-bonds were detected between the protein residues TYR115 and THR115 and H-N-H bond. Table 10 provides docking parameters. Figures 13 and 14 displays docked interactions and the conformations with the lowest binding energies are considered the ones that are best-docked. As can be seen from the results, the antiviral protein had a good affinity sand the lowest binding energy(BE), indicating good antiviral activity of the chosen compound. So, it can be concluded that the compound has better antiviral activity than standard drug which is used to treat anti viral disease and can be considered as a prospective pharmaceutical medication.

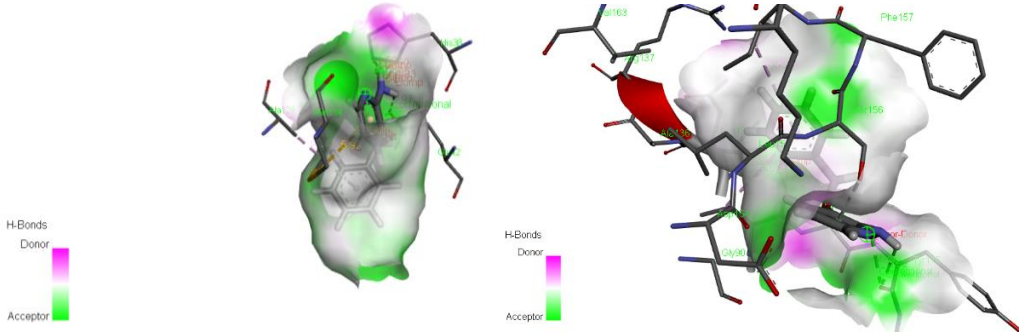

Figure 13 A, B . 3D Top binding pose of proteins (5XUI, 4IIT)

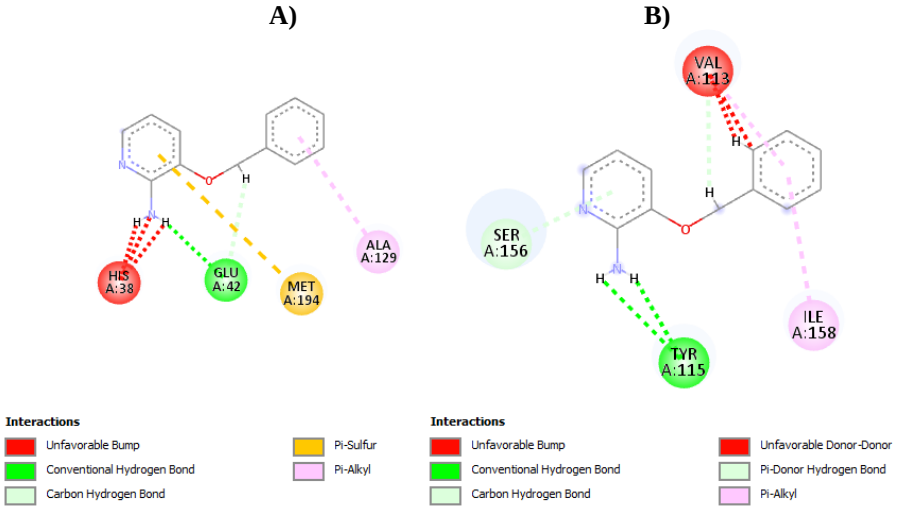

Figure 14 A,B. 2D Top binding pose of proteins ((5XUI, 4IIT))

Table 10. The interaction energy analysis of 2-amino-3-benzyloxypyridine with targeted protein

Properties	Protein ID	**Residue**	**Interaction**	**Bond Distance Å**	**Inhibiton Constant (micro molar)**	**Binding Energy (kcal/ mol)**	**RMSD**
Anti-Viral	5XUI	GLU42 GLU42 MET194 ALA129 GLU42	Conventional hydrogen bond π-Sulphur π-Sulphur π-Alkyl Carbon hydrogen bond Alkyl	3.10 4.53 4.55 2.43 4.80 2.16	67.76	-9.10	28.336
	4IIT	TYR115 THR115 SER156 ILE158 VAL113	Conventional hydrogen bond Conventional Hydrogen bond Carbon Hydrogen Bond Carbon Hydrogen Bond π-Donar Hydrogen bond	3.27 2.39 4.42 2.14 1.56	109.07	-6.18	40.438

4. Conclusion

The PES approach was used in this work to determine the most stable conformer of 2A3BP. Quantum chemical computations were employed to perform a thorough evaluation of the spectroscopical properties of the 2A3BP molecule under discussion. Bond lengths and

bond angles were all computed to have ideal geometric properties. The optimized shape of the structure demonstrates the existence of hydrogen bonding. NBO scrutiny approves the existence of intra-molecular hydrogen bonding. Band gap suggests the potential of inter-molecular exchange of charges, making the molecule a suitable pharmacological component. UV-Vis spectra measured theoretically were compared to solvents. It became apparent that the transition had the largest absorbance band at 305 nm. As a consequence, the present research provides exact vibrational assignments, chemical shifts, and physical molecular properties. The 2A3BP's surface has been exposed to MESP, ELF, and LOL in investigations in order to examine the arrangement of electrons and reactive regions. Furthermore, the molecular docking finding implies that it would have strong anti-microbial action.

References

1. Zhan, P., Pannecouque, C., De Clercq, E., & Liu, X. (2016). Anti-HIV drug discovery and development: current innovations and future trends: miniperspective. *Journal of medicinal chemistry*, *59*(7), 2849-2878.
2. Kaiser, J. P., Feng, Y., & Bollag, J. M. (1996). Microbial metabolism of pyridine, quinoline, acridine, and their derivatives under aerobic and anaerobic conditions. *Microbiological reviews*, *60*(3), 483-498.
3. Patil, P., Sethy, S. P., Sameena, T., & Shailaja, K. (2013). Pyridine and its biological activity: a review. *Asian Journal of Research in Chemistry*, *6*(10), III.
4. Combrinck, J. M., Mabotha, T. E., Ncokazi, K. K., Ambele, M. A., Taylor, D., Smith, P. J., ... & Egan, T. J. (2013). Insights into the role of heme in the mechanism of action of antimalarials. *ACS chemical biology*, *8*(1), 133-137.
5. Desoize, B. (2004). Metals and metal compounds in cancer treatment. *Anticancer Research*, *24*(3A), 1529-1544.
6. Ali, I., Asim, M., & Khan, T. A. (2012). Low cost adsorbents for the removal of organic pollutants from wastewater. *Journal of environmental management*, *113*, 170-183.
7. Dhingra, N., Singh, J. B., & Singh, H. L. (2022). Synthesis, spectroscopy, and density functional theory of organotin and organosilicon complexes of bioactive ligands containing nitrogen, sulfur donor atoms as antimicrobial agents: in vitro and in silico studies. *Dalton Transactions*, *51*(22), 8821-8831.
8. Suvitha, A., Periandy, S., Boomadevi, S., & Govindarajan, M. (2014). Vibrational frequency analysis, FT-IR, FT-Raman, ab initio, HF and DFT studies, NBO, HOMO–LUMO and electronic structure calculations on pycolinaldehyde oxime. *Spectrochimica Acta Part A: Molecular and Biomolecular Spectroscopy*, *117*, 216-224.
9. Agarwal, N., Verma, I., Siddiqui, N., & Javed, S. (2021). Experimental spectroscopic and quantum computational analysis of pyridine-2, 6-dicarboxalic acid with molecular docking studies. *Journal of Molecular Structure*, *1245*, 131046.
10. Freindorf, M., Kraka, E., & Cremer, D. (2012). A comprehensive analysis of hydrogen bond interactions based on local vibrational modes. *International Journal of Quantum Chemistry*, *112*(19), 3174-3187.
11. Barone, V., Alessandrini, S., Biczysko, M., Cheeseman, J. R., Clary, D. C., McCoy, A. B., ... & Puzzarini, C. (2021). Computational molecular spectroscopy. *Nature Reviews Methods Primers*, *1*(1), 38.
12. Sherrill, C. D. (2010). Frontiers in electronic structure theory. *The Journal of chemical physics*, *132*(11).
13. Stuart, S. J., Tutein, A. B., & Harrison, J. A. (2000). A reactive potential for hydrocarbons with intermolecular interactions. *The Journal of chemical physics*, *112*(14), 6472-6486.
14. Sosa, G. L., Peruchena, N. M., Contreras, R. H., & Castro, E. A. (2002). Topological and NBO analysis of hydrogen bonding interactions involving C–H··· O bonds. *Journal of Molecular structure: THEOCHEM*, *577*(2-3), 219-228.
15. Hiscocks, J., & Frisch, M. J. (2009). *Gaussian 09: IOps Reference*. M. Caricato, & M. J. Frisch (Eds.). Wallingford, CT, USA: Gaussian.
16. Jamroz, M. H. (2004). Vibrational energy distribution analysis VEDA 4.
17. Jamróz, M. H. (2013). Vibrational energy distribution analysis (VEDA): scopes and limitations. *Spectrochimica Acta Part A: Molecular and Biomolecular Spectroscopy*, *114*, 220-230.
18. Pilli, S. R., Banerjee, T., & Mohanty, K. (2015). HOMO–LUMO energy interactions between endocrine disrupting chemicals and ionic liquids using the density functional theory: Evaluation and comparison. *Journal of Molecular Liquids*, *207*, 112-124.
19. O'boyle, N. M., Tenderholt, A. L., & Langner, K. M. (2008). Cclib: a library for package-independent computational chemistry algorithms. *Journal of computational chemistry*, *29*(5), 839-845.
20. Rijal, R., Sah, M., & Lamichhane, H. P. (2023). Molecular simulation, vibrational spectroscopy and global reactivity descriptors of pseudoephedrine molecule in different phases and states. *Heliyon*, *9*(3).
21. Lu, T., & Chen, F. (2012). Multiwfn: A multifunctional wavefunction analyzer. *Journal of computational chemistry*, *33*(5), 580-592.
22. Mishra, S., & Dahima, R. (2019). In vitro ADME studies of TUG-891, a GPR-120 inhibitor using SWISS ADME predictor. *Journal of drug delivery and therapeutics*, *9*(2-s), 366-369.
23. Rizvi, S. M. D., Shakil, S., & Haneef, M. (2013). A simple click by click protocol to perform docking: AutoDock 4.2 made easy for non-bioinformaticians. *EXCLI journal*, *12*, 831.
24. Kowalczyk, T., Yost, S. R., & Voorhis, T. V. (2011). Assessment of the ΔSCF density functional theory

approach for electronic excitations in organic dyes. *The Journal of chemical physics*, *134*(5).

25. Wang, Y., Lv, J., Zhu, L., & Ma, Y. (2012). CALYPSO: A method for crystal structure prediction. *Computer Physics Communications*, *183*(10), 2063-2070.
26. Güleryüz, C., Sumrra, S. H., Mohyuddin, A., Hassan, A. U., & Dahshan, A. (2024). Theoretical calculations of nonlinear optical responses for interpreting nonconjugated molecular systems to affect non-optimal properties. *Spectrochimica Acta Part A: Molecular and Biomolecular Spectroscopy*, 125244.
27. Devitt, G., Howard, K., Mudher, A., & Mahajan, S. (2018). Raman spectroscopy: an emerging tool in neurodegenerative disease research and diagnosis. *ACS chemical neuroscience*, *9*(3), 404-420.
28. Sathyanarayana, D. N. (2015). *Vibrational spectroscopy: theory and applications*. New Age International.
29. Mishma, J. C., Jothy, V. B., Irfan, A., Narayana, B., Kodlady, S. N., & Muthu, S. (2023). Solvent potential effects (topological aspects, electron excitation), spectral characterization and biological attributes of NLO active 1-(2, 4-dinitrophenyl)-2-((E)-3-phenylallylidene) hydrazine: Multiple anti tuberculosis agent. *Journal of Molecular Liquids*, *376*, 121439.
30. Loroño, M., Boudon, V., Loete, M., Rotger, M., Bourgeois, M. T., Didriche, K., ... & Petrova, T. M. (2010). High-resolution spectroscopy and preliminary global analysis of C–H stretching vibrations of C2H4 in the 3000 and 6000 cm− 1 regions. *Journal of Quantitative Spectroscopy and Radiative Transfer*, *111*, 2151-2159.
31. Rawat, B., & Garg, A. P. (2021). Characterization of phytochemicals isolated from cucurbita pepo seeds using uv-vis and ftir spectroscopy. *Plant Archives (09725210)*, *21*(1).
32. Arjunan, V., Marchewka, M. K., Raj, A., Yang, H., & Mohan, S. (2015). Structural and vibrational spectral investigations of melaminium glutarate monohydrate by FTIR, FT-Raman and DFT methods. *Spectrochimica Acta Part A: Molecular and Biomolecular Spectroscopy*, *135*, 540-550.
33. Diem, M. (2015). *Modern vibrational spectroscopy and micro-spectroscopy: theory, instrumentation and biomedical applications*. John Wiley & Sons.
34. Sun, Q. (2009). The Raman OH stretching bands of liquid water. *Vibrational Spectroscopy*, *51*(2), 213-217.
35. Fuson, N., Josien, M. L., Powell, R. L., & Utterback, E. (1952). The NH stretching vibration and NH–N hydrogen bonding in several aromatic compounds. *The Journal of Chemical Physics*, *20*(1), 145-152.
36. Mishma, J. C., Jothy, V. B., Muthu, S., & Irfan, A. (2022). Bonding nature, nucleophilic reactivity and electron excitation of NLO active 2, 6 dichloroindophenol sodium salt (polar and non polar solvents) with topology analysis-bacterial pathogens study. *Journal of Molecular Liquids*, *367*, 120533.
37. Rekha, S., Tamilselvan, S., Vetrivelan, V., Mishma, J. C., Kadaikunnan, S., Abbas, G., & Muthu, S. (2023). Effect of different solvents, molecular level vibrational energies, electronic, electrostatic, donar-acceptor and pharmaceutical studies on 3-Methoxy phenyl acetonitrile-anti depressant agent. *Journal of Molecular Liquids*, 122308.
38. Mani, N., Nicksonsebastin, D., Prasath, M., Mishma, J. C., Kadaikunnan, S., Abbas, G., & Muthu, S. (2023). Potential energy surface, effect of solvents in molecular level, experimental spectra (FTIR, Raman, UV–visible & NMR), electronic, and dynamics simulation of isobavachalcone–Anti tuberculosis agent. *Journal of Molecular Liquids*, 123465.
39. Rahuman, M. H., Muthu, S., Raajaraman, B. R., Raja, M., & Umamahesvari, H. (2020). Investigations on 2-(4-Cyanophenylamino) acetic acid by FT-IR, FT-Raman, NMR and UV-Vis spectroscopy, DFT (NBO, HOMO-LUMO, MEP and Fukui function) and molecular docking studies. *Heliyon*, *6*(9).
40. Islam, M. M., & Strachan, A. (2017). Decomposition and reaction of polyvinyl nitrate under shock and thermal loading: a ReaxFF reactive molecular dynamics study. *The Journal of Physical Chemistry C*, *121*(40), 22452-22464.
41. Gentili, P. L., Ortica, F., & Favaro, G. (2008). Static and dynamic interaction of a naturally occurring photochromic molecule with bovine serum albumin studied by UV− visible absorption and fluorescence spectroscopy. *The Journal of Physical Chemistry B*, *112*(51), 16793-16801.
42. Vennila, M., Rathikha, R., Muthu, S., Jeelani, A., & Irfan, A. (2022). Theoretical structural analysis (FT-IR, FT-R), solvent effect on electronic parameters NLO, FMO, NBO, MEP, UV (IEFPCM model), Fukui function evaluation with pharmacological analysis on methyl nicotinate. *Computational and Theoretical Chemistry*, *1217*, 113890.
43. Fattah, M. F. A. (2020). *SOFT X-RAY SPECTROSCOPY STUDY of WIDE BAND GAP SEMICONDUCTORS-M2PN3 (M= Mg, Zn) and BP3N6* (Doctoral dissertation, University of Saskatchewan).
44. Link, S., & El-Sayed, M. A. (2000). Shape and size dependence of radiative, non-radiative and photothermal properties of gold nanocrystals. *International reviews in physical chemistry*, *19*(3), 409-453.
45. Sheikhi, M., Balali, E., & Lari, H. (2016). Theoretical investigations on molecular structure, NBO, HOMO-LUMO and MEP analysis of two crystal structures of N-(2-benzoyl-phenyl) oxalyl: A DFT study. *Journal of Physical & Theoretical Chemistry*, *13*(2), 155-169.
46. Koritsanszky, T. S., & Coppens, P. (2001). Chemical applications of X-ray charge-density analysis. *Chemical reviews*, *101*(6), 1583-1628.

47. Muthu, S., & Porchelvi, E. E. (2013). FTIR, FT-RAMAN, NMR, spectra, normal co-ordinate analysis, NBO, NLO and DFT calculation of N, N-diethyl-4-methylpiperazine-1-carboxamide molecule. *Spectrochimica Acta Part A: Molecular and Biomolecular Spectroscopy*, *115*, 275-286.
48. Glendening, E. D., Landis, C. R., & Weinhold, F. (2012). Natural bond orbital methods. *Wiley interdisciplinary reviews: computational molecular science*, *2*(1), 1-42.
49. de Lange, J. H., van Niekerk, D. M., & Cukrowski, I. (2019). Quantifying individual (anti) bonding molecular orbitals' contributions to chemical bonding. *Physical Chemistry Chemical Physics*, *21*(37), 20988-20998.
50. Gangadharan, R., & Sampath Krishnan, S. (2014). Natural Bond Orbital (NBO) population analysis of 1-azanapthalene-8-ol. *Acta Physica Polonica A*, *125*(1), 18-22.
51. Alabugin, I. V., Bresch, S., & dos Passos Gomes, G. (2015). Orbital hybridization: a key electronic factor in control of structure and reactivity. *Journal of Physical Organic Chemistry*, *28*(2), 147-162.
52. Dege, N., Gökce, H., Doğan, O. E., Alpaslan, G., Ağar, T., Muthu, S., & Sert, Y. (2022). Quantum computational, spectroscopic investigations on N-(2-((2-chloro-4, 5-dicyanophenyl) amino) ethyl)-4-methylbenzenesulfonamide by DFT/TD-DFT with different solvents, molecular docking and drug-likeness researches. *Colloids and Surfaces A: Physicochemical and Engineering Aspects*, *638*, 128311.
53. Basha, S. J., Chamundeeswari, S. V., Muthu, S., & Raajaraman, B. R. (2019). Quantum computational, spectroscopic investigations on 6-aminobenzimidazole by DFT/TD-DFT with different solvents and molecular docking studies. *Journal of Molecular Liquids*, *296*, 111787.
54. Arulaabaranam, K., Muthu, S., Mani, G., & Irfan, A. (2022). Molecular Structure, Spectroscopic Assessment, PDOS, Topology Evaluation and Docking Studies of 2-Chloro-5-nitrobenzophenone. *Analytical Chemistry Letters*, *12*(2), 198-220.
55. Mishma, J. C., Jothy, V. B., Irfan, A., Narayana, B., & Muthu, S. (2023). Role of solvents in molecular level interaction, reactivity and spectral characterisation of 2-Amino-3-(((E)-4-(dimethylamino) benzylidene) amino) maleonitrile: Anti depressant agent. *Journal of Molecular Liquids*, *389*, 122937.
56. Reeda, V. J., Jothy, V. B., Asif, M., Nasibullah, M., Alharbi, N. S., Abbas, G., & Muthu, S. (2023). Synthesis, solvent polarity (polar and nonpolar), structural and electronic properties with diverse solvents and biological studies of (E)-3-((3-chloro-4-fluorophenyl) imino) indolin-2-one. *Journal of Molecular Liquids*, *380*, 121709.
57. Reeda, V. J., Sakthivel, S., Divya, P., Javed, S., & Jothy, V. B. (2023). Conformational Stability, Quantum Computational (DFT), Vibrational, Electronic and Non-covalent Interactions (QTAIM, RDG and IGM) of Antibacterial Compound N-(1-Naphthyl) ethylenediamine dihydrochloride. *Journal of Molecular Structure*, 137043.
58. Kumar, B. A., Vetrivelan, V., Ramalingam, G., Manikandan, A., Viswanathan, S., Boomi, P., & Ravi, G. (2022). Computational studies and experimental fabrication of DSSC device assembly on 2D-layered TiO2 and MoS2@ TiO2 nanomaterials. Physica B: Condensed Matter, 633, 413770
59. Manjusha, P., Prasana, J. C., Muthu, S., & Rizwana, B. F. (2020). Spectroscopic elucidation (FT-IR, FT-Raman and UV-visible) with NBO, NLO, ELF, LOL, drug likeness and molecular docking analysis on 1-(2-ethylsulfonylethyl)-2-methyl-5-nitro-imidazole: An antiprotozoal agent. Computational Biology and Chemistry, 88, 107330.
60. Janani, S., Rajagopal, H., Muthu, S., Aayisha, S., & Raja, M. (2021). Molecular structure, spectroscopic (FT-IR, FT-Raman, NMR), HOMO-LUMO, chemical reactivity, AIM, ELF, LOL and Molecular docking studies on 1-Benzyl-4-(N-Boc-amino) piperidine. *Journal of Molecular Structure*, *1230*, 129657.
61. Warshel, A. (2002). Molecular dynamics simulations of biological reactions. Accounts of chemical research, 35(6), 385-395.
62. Jemai, M., Issaoui, N., Roisnel, T., Kazachenko, A. S., Al-Dossary, O. M., & Marouani, H. (2023). Solvent–solute and non-covalent interactions on bis (4-Piperidinonium ethyl ketal) oxalate compound: DFT calculations and in silico drug-target profiling. Journal of Molecular Liquids, 391, 123261.
63. Jeelani, A., Muthu, S., Ramesh, P., & Irfan, A. (2022). Experimental spectroscopic, molecular structure, electronic solvation, biological prediction and topological analysis of 2, 4, 6-tri (propan-2-yl) benzenesulfonyl chloride: An antidepressant agent. *Journal of Molecular Liquids*, *358*, 119166.
64. Günther, D., Boto, R. A., Contreras-Garcia, J., Piquemal, J. P., & Tierny, J. (2014). Characterizing molecular interactions in chemical systems. IEEE transactions on visualization and computer graphics, 20(12), 2476-2485.
65. Hobza, P., & Müller-Dethlefs, K. (2010). Non-covalent interactions: theory and experiment (Vol. 2). Royal Society of Chemistry.
66. Suga, K., Fujita, S., Yamada, H., & Fujihira, M. (1990). Comparison between intra-and intermolecular photoinduced electron transfer reactions of micelle-solubilized substances. Bulletin of the Chemical Society of Japan, 63(12), 3369-3375.
67. Kümmerer, K. (2009). The presence of pharmaceuticals in the environment due to human use–present knowledge and future challenges. Journal of environmental management, 90(8), 2354-2366.

68. Kaczorowski, G. J., McManus, O. B., Priest, B. T., & Garcia, M. L. (2008). Ion channels as drug targets: the next GPCRs. The Journal of general physiology, 131(5), 399-405.
69. Jeelani, A., Muthu, S., Raajaraman, B. R., & Sevvanthi, S. (2020). Spectroscopic, quantum chemical calculations, and molecular docking analysis of 3-Chlorophenyl boronic acid. *Spectroscopy Letters*, *53*(10), 778-792.
70. Kolodziejczyk-Czepas, J., Sieradzka, M., Moniuszko-Szajwaj, B., Pecio, Ł., Ponczek, M. B., Nowak, P., & Stochmal, A. (2017). Bufadienolides from Kalanchoe daigremontiana as thrombin inhibitors—In vitro and in silico study. International journal of biological macromolecules, 99, 141-150.
71. Martial, C., Cassol, H., Charland-Verville, V., Pallavicini, C., Sanz, C., Zamberlan, F., ... & Tagliazucchi, E. (2019). Neurochemical models of near-death experiences: A large-scale study based on the semantic similarity of written reports. Consciousness and cognition, 69, 52-69.
72. Chandrasekaran, B., Abed, S. N., Al-Attraqchi, O., Kuche, K., & Tekade, R. K. (2018). Computer-aided prediction of pharmacokinetic (ADMET) properties. In Dosage form design parameters (pp. 731-755). Academic Press.
73. Kowalska, M., Fijałkowski, Ł., & Nowaczyk, A. (2018). The biological activity assessment of potential drugs acting on cardiovascular system using Lipinski and Veber Rules. Journal of Education, Health and Sport, 8(12), 184-191.
74. Chen, X., Li, H., Tian, L., Li, Q., Luo, J., & Zhang, Y. (2020). Analysis of the physicochemical properties of acaricides based on Lipinski's rule of five. Journal of computational biology, 27(9), 1397-1406.
75. Khemalapure, S. S., Hiremath, S. M., Basanagouda, M. M., Hiremath, C. S., Koppal, V. V., & Jeyaseelan, S. C. (2023). Design, Vibrational and Fluorescence Spectroscopic Properties, and Molecular Docking Studies of 3-(5-Bromobenzofuran-3-ylmethyl)-5-(4-methoxyphenyl)-4H-[1, 2, 4]-triazole by Experimental and Density Functional Theory Methods. ChemistrySelect, 8(17), e202300428.
76. Morris, G. M., & Lim-Wilby, M. (2008). Molecular docking. *Molecular modeling of proteins*, 365-382.
77. Filimonov, D. A., Lagunin, A. A., Gloriozova, T. A., Rudik, A. V., Druzhilovskii, D. S., Pogodin, P. V., & Poroikov, V. V. (2014). Prediction of the biological activity spectra of organic compounds using the PASS online web resource. *Chemistry of Heterocyclic Compounds*, *50*, 444-457.
78. Pagadala, N. S., Syed, K., & Tuszynski, J. (2017). Software for molecular docking: a review. *Biophysical reviews*, *9*, 91-102.
79. Rose, P. W., Bi, C., Bluhm, W. F., Christie, C. H., Dimitropoulos, D., Dutta, S., ... & Bourne, P. E. (2012). The RCSB Protein Data Bank: new resources for research and education. *Nucleic acids research*, *41*(D1), D475-D482.
80. Bielenica, A., Beegum, S., Mary, Y. S., Mary, Y. S., Thomas, R., Armaković, S., ... & Van Alsenoy, C. (2020). Experimental and computational analysis of 1-(4-chloro-3-nitrophenyl)-3-(3, 4-dichlorophenyl) thiourea. *Journal of Molecular Structure*, *1205*, 127587.